Planar laser imaging and modeling of matrix-assisted pulsed-laser evaporation direct write in the bubble regime

Brent R. Lewis, Edward C. Kinzel, Normand M. Laurendeau,[a] Robert P. Lucht, and Xianfan Xu
School of Mechanical Engineering, Purdue University, West Lafayette, Indiana 47907

(Received 14 November 2005; accepted 28 May 2006; published online 10 August 2006)

A combination of planar laser imaging and theoretical modeling has been used to examine matrix-assisted pulsed-laser evaporation direct write (MAPLE-DW) in the bubble regime. MAPLE-DW is a method for patterning substrates via laser-initiated forward transfer of an organic fluid containing metallic particles and coated on a transparent support. For our conditions, best deposition of a silver-based, thick-film ink was found to occur when laser-initiated vaporization forces the ink outward as a bubble. Planar laser imaging was used to monitor bubble growth as a function of time for three different ink films with nominal thicknesses of 12, 25, and 50 μm and two laser beam diameters of 30 and 60 μm. From these measurements, correlations were developed for predicting the maximum height and velocity of bubbles via three known process variables: laser energy, ink thickness, and beam diameter. Further insight on the physics of the MAPLE-DW process was obtained by developing a theoretical model for bubble growth based on a simple force balance associating vapor-pocket pressure and viscous forces. Primary parameters specifying the subsequent differential equation were related to the above process variables. Numerical solutions to the differential equation were used to predict successfully bubble growth versus time for the conditions analyzed in the imaging experiments. © *2006 American Institute of Physics*.
[DOI: 10.1063/1.2234542]

I. INTRODUCTION

Demands for smaller feature sizes and rapid prototyping have prompted investigations of matrix-assisted pulsed-laser evaporation direct write (MAPLE-DW) as a potential process for laser-based microfabrication. MAPLE-DW can be used to deposit a single electronic component or a suitable array of conformal devices over almost any surface at ambient conditions.[1] Furthermore, the versatility of MAPLE-DW permits the manufacture of microelectronic components across many fields, including commercial appliances, common household fixtures, chemical sensors, biosensor arrays, and high-frequency devices.[2] Not only are small devices being installed into larger systems, but complete electrochemical systems are being created at the microscale using fully integrated miniature power sources.[3] Because applications for microelectronic devices are constantly emerging, fundamental mechanisms controlling the MAPLE-DW process continue to warrant research investigations.

Applying time-resolved optical microscopy to MAPLE-DW, Young *et al.*[4] previously identified three distinct regimes of ink response ordered by rising laser fluence: subthreshold, jetting, and plume. Moreover, laser absorption during the process was related to the formation of a vapor pocket at the ink-quartz interface, as shown in Fig. 1. The vapor pocket expands and deforms the ink layer on the associated ribbon, producing one of the three response regimes.

In this paper, we employ planar laser imaging to characterize more completely the interaction between laser absorption and subsequent outward expansion of ink, as commonly used for microelectronics manufacturing. Images of the expansion process are obtained by pulsing a sheet of light created via a Nd:YAG (yttrium aluminum garnet) laser. This sheet illuminates the flow field from the side, providing transient images of the rheological fluid leaving the ribbon. Similar to the basic conclusion of Young *et al.*[4], initial work identified three regimes of ablated ink flows: bubble, jet, and plume. These regimes are shown in Fig. 2. However, contrary to the suggestion of Young *et al.*,[4] we obtained smaller feature sizes and more repeatable deposition when operating

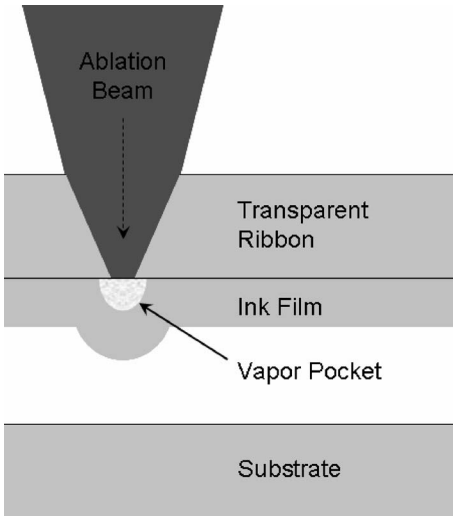

FIG. 1. Schematic diagram of MAPLE-DW process.

[a]Author to whom correspondence should be addressed; electronic mail: laurende@ecn.purdue.edu

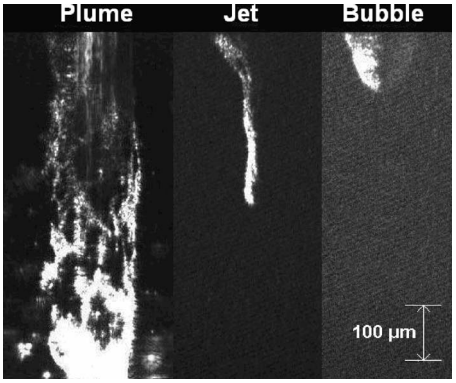

FIG. 2. Pictorial views of plume, jet, and bubble classifications for ink-film response.

in the bubble regime as opposed to the jet regime. The primary reason for this behavior appears to be the inconsistent shape and high speed of the fluid jet that leaves the ribbon at fluences beyond the bubble regime. Based on this result, we focus here on planar imaging of the MAPLE-DW process solely within the bubble regime.

Images obtained during this investigation were analyzed and compared based on the primary process parameters of laser energy, beam diameter, and ink-film thickness. To enhance our understanding of bubble formation, a theoretical model was also developed using a simple force balance. The resulting differential equation can ultimately be related to a combination of intermediate variables and the above process parameters. Numerical solutions to the characteristic differential equation were applied to actual measurements of bubble growth versus time. To control accurately the size and growth of bubbles, we investigated relations between measured bubble characteristics and different combinations of ink thickness, beam diameter, and ablation energy. Correlations to bubble growth data are provided to enable predictions of maximum bubble height, bubble radius, and maximum bubble velocity.

II. EXPERIMENTAL SETUP

A detailed schematic of the experimental apparatus is shown in Fig. 3. Vaporization of ink at the interface is achieved by employing a Spectra-Physics 7300 Nd:YLF laser-diode module. The 1047 nm diode output varies in frequency from 1 to 10 000 Hz, with an adjustable power up to 2 W and a pulse width of 20 ns. The Nd:YLF output beam is expanded by a factor of 10 using spherical lenses with focal lengths of 30 and 300 mm. The laser energy can be varied by using a 1064 nm half-wave plate and a thin-film plate polarizer. The effective beam diameter at the interface is controlled by adjusting the position of a 75 mm spherical focusing lens.

A frequency-doubled Continuum Surelite III Nd:YAG laser is used to illuminate the vaporization process. At 532 nm, this laser provides an energy of 300 mJ/pulse at a repetition rate of 10 Hz. To illuminate the flow field, a sheet of light is created with two lenses. A cylindrical lens diverges

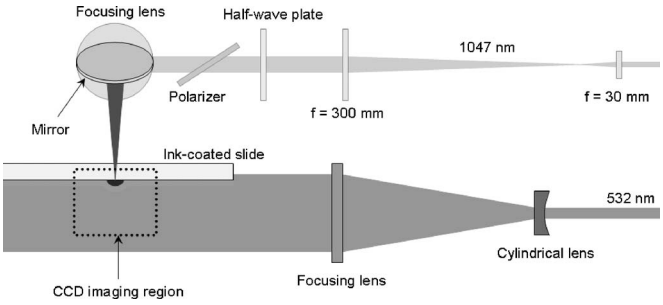

FIG. 3. Experimental setup for planar laser imaging of MAPLE-DW process.

the Nd:YAG beam along the vertical axis. A spherical focusing lens focuses the beam along the horizontal axis and recollimates the beam along its vertical axis.

Images are captured with an Andor iXon electron-multiplying charge-coupled device (EMCCD) camera, which has a 512×512 CCD array and a pixel size of 16 μm. An objective lens with adjustable magnification between 2.5 and 10 provides a viewable field between 0.82 and 3.28 mm square. The shortest available gate time of the iXon camera is 20 μs. However, this camera is capable of taking data at the laser repetition rate of 10 Hz, enabling fast and efficient data collection. Two Stanford Research Systems DG535 delay generators are employed to ensure precise delays between the onset of vaporization and sequential images of bubble growth.

The ink employed for this research is DuPont QS300, a conductive paste developed for screen printing that contains silver microparticles. While the viscosity of QS300 actually varies with shear rate, its appearance at room temperature is that of a thick gray paste. Moreover, its high viscosity at low speeds prevents QS300 from smoothing out naturally when coated onto ribbons with a 5 μm wire roller. Therefore, ink films were created by placing a droplet of ink at one end of a soda-lime glass slide between two metal shims. A glass rod was then pulled across the two shims, creating a flat layer of ink at nearly the same thickness as that of the shims.

III. ANALYTICAL MODEL FOR BUBBLE GROWTH

A one-dimensional model was developed so as to provide a simple physical explanation for both laser-induced evaporation and subsequent bubble expansion. The model begins with a fundamental force balance, as shown in Fig. 4. We assume that the pressure created in the vapor pocket and the surrounding viscous response constitute the only two forces acting on the column of ink, as given by

$$F_P = (P - P_{\text{atm}})A_C \tag{1}$$

and

$$F_V = -kv, \tag{2}$$

respectively. The pressure force, given by Eq. (1), results from the difference between the pressure created inside the vapor pocket and atmospheric pressure acting on the ink surface. The pressure inside the vapor pocket changes as the pocket forces ink away from the ribbon. These pressure forces act on the circular area of the ink column, $A_C=\pi R^2$.

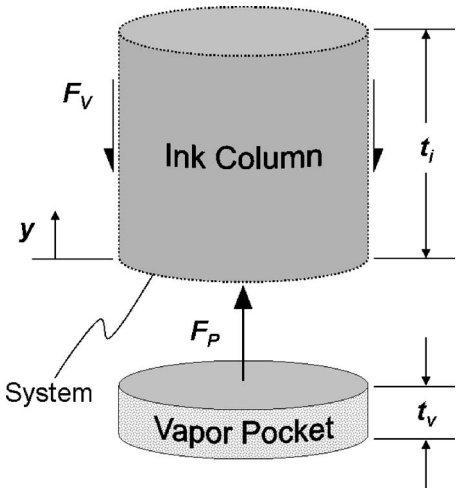

FIG. 4. Force diagram of ink-column system showing vapor pocket.

The viscous force, given by Eq. (2), is assumed to be directly proportional to the average velocity of the ink column, v. The proportionality constant k can subsequently be related to the contact area between the cylindrical column and its surrounding ink. Therefore, we replace k with a new viscous-force constant k_C ($m^{-2}\,s^{-1}$) given by

$$k_C = \frac{k}{2\pi R t_i}, \tag{3}$$

where R is the common radius of the ink column and vapor pocket (μm), while t_i is the nominal ink thickness (μm). For simplicity, we take the contact area between the rigid-ink cylinder and its surrounding ink to be constant during the vaporization process.

Applying Newton's second law to the viscous and pressure forces, we may derive a characteristic differential equation for the bubble height y above the ink layer, given by

$$y'' + \frac{2k_C}{\rho_i R} y' - \frac{P_0 t_{v0}}{\rho_i t_i} y^{-1} = -\frac{P_{\text{atm}}}{\rho_i t_i}, \tag{4}$$

where ρ_i is the ink density (kg/m^3), P_0 is the initial vapor-pocket pressure (Pa), t_{v0} is the initial vapor-pocket thickness (μm), and P_{atm} is the atmospheric pressure (Pa). Recall that our specified process parameters are the nominal ink thickness, laser-beam diameter, and ablation energy. Because the viscous-force constant, ink density, ink column radius, initial vapor-pocket thickness, and initial vapor-pocket pressure are unknown, we require further assumptions to relate these intermediate variables to the above process parameters.

The viscous-force constant and ink density are assumed to be constant throughout all variations of ink thickness, beam diameter, and ablation energy. The actual geometry is clearly not a cylinder, as evidenced by bubble pictures. Furthermore, bubble growth is monitored via the tip of a parabolic bubble, which we attempt to match with an entire cylinder. Therefore, we expect a model density of perhaps half the actual ink density, as much less mass is moving outward for the actual bubbles. As will be discussed later, the fluid density determined by fitting the model to experimental data is actually considerably lower than even this expected density.

Another critical assumption is negligible heat transfer from the vapor pocket during the process, when in reality some energy must be lost in the radial direction. The vapor trapped by the ink is also assumed not to condense throughout its expansion, ruling out the possibility of an associated reduction in pressure. Although thermal effects might still be operative, our overall adiabatic assumption is reasonable given the extremely rapid processes of evaporation and bubble growth.

When the bubble stops moving, the acceleration and velocity terms of Eq. (4) are zero. Therefore, the final bubble height is given by

$$y_{ss} = \frac{P_0 t_{v0}}{P_{\text{atm}}}. \tag{5}$$

We thus find from Eq. (5) that the final bubble height y_{ss} depends only on the initial vapor-pocket pressure P_0 and the initial vapor-pocket thickness t_{v0}. Although absolute values of P_0 and t_{v0} are unknown, their product can be calculated directly by multiplying the experimental height y_{ss} by P_{atm}. On this basis, $P_0 t_{v0}$ can be determined via curve fitting a single data set; further values can then be determined by invoking a scaling ratio based on process variables. Scaling ratios for vapor-pocket thickness and pressure are discussed in Sec. III B.

A. Vapor-pocket radius

The radius of the ink column can be related quite easily to the beam diameter and laser energy. If the energy within the beam is distributed according to a Gaussian profile, then the local fluence F can be described as a function of radius r given by

$$F = F_0 \exp\left(-\frac{r^2}{2\sigma^2}\right), \tag{6}$$

where σ is the standard deviation of the spatial profile. The nominal fluence F_N can be calculated from the beam diameter d and the pulse energy E by

$$F_N = \frac{4E}{\pi d^2}. \tag{7}$$

For this study, we define the beam diameter as the distance between lateral positions of a razor edge at which the transmitted energy drops from 90% to 10% of its full-scale value, which corresponds to a radial distance of 2.564σ.[5] The centerline fluence can thus be calculated directly from the nominal fluence by

$$F_0 = 1.28 F_N. \tag{8}$$

Assuming that the vapor-pocket radius can be determined by the radial position at which the local fluence passes above a threshold F_t, the radius R at which this threshold is surpassed can be expressed as

$$R = \frac{d\sqrt{2\ln(F_0/F_t)}}{2.564}. \tag{9}$$

We presume a threshold fluence $F_t = 0.15$ J/cm^2 for all calculations, because this value defines the lowest bubble-producing fluence measured during the experiments of this investigation. On this basis, Eq. (9) can be used to determine the vapor-pocket radius for any specified beam energy and diameter.

B. Vapor-pocket thickness and pressure

According to Beer's law, incoming energy is absorbed such that its value as a function of ink-film depth y is given by

$$E(y) = E_0 \exp(-\mu_t y), \tag{10}$$

where E_0 is the initial beam energy and μ_t is an attenuation coefficient. Although we cannot directly calculate the attenuation coefficient, an exact value is not necessary because of the relation between initial vapor-pocket thickness and final bubble height given by Eq. (5). We thus assign a baseline vapor-pocket thickness $t_{v0,a}$ of 1 μm to the previous data set chosen for curve fitting. Employing Eq. (10) for this baseline vapor-pocket thickness, defined as the depth at which the laser energy has decayed to its threshold value E_t, the initial thickness of the vapor pocket for subsequent data sets can be determined from

$$t_{v0,b} = t_{v0,a}\frac{\ln(E_b/E_t)}{\ln(E_a/E_t)}, \tag{11}$$

where E_a is the measured beam energy for the curve-fitted data set. Based on a fluence threshold, $F_t = 0.15$ J/cm^2, we find that the 30 and 60 μm beam diameters yield equivalent energy thresholds of 1.0 and 4.2 μJ, respectively.

The final unknown required for solving Eq. (4) is the initial vapor-pocket pressure P_0. Fortunately, once the initial vapor-pocket thickness has been determined, the initial vapor-pocket pressure can be easily calculated from Eq. (5). However, a problem arises when attempting to determine how the magnitude of this pressure changes with laser energy, ink thickness, and beam diameter. Assuming that these variables all affect the initial vapor-pocket pressure, we suppose that an unknown initial vapor-pocket pressure $P_{0,b}$ can be determined from that based on curve-fitted data $P_{0,a}$ through

$$P_{0,b} = P_{0,a}\left(\frac{E_b}{E_a}\right)\left(\frac{t_{i,b}}{t_{i,a}}\right)^m\left(\frac{d_b}{d_a}\right)^n, \tag{12}$$

where m and n are variable exponents for ink thickness and beam diameter, respectively. Although a least-squares fit was used to determine m and n, this procedure is not the same as fitting the initial pressure directly to final bubble heights via Eq. (5). The difference is that the preferred method used here provides a correlation between initial vapor-pocket pressure and known process variables, which could be used in future work. The final relation is given by

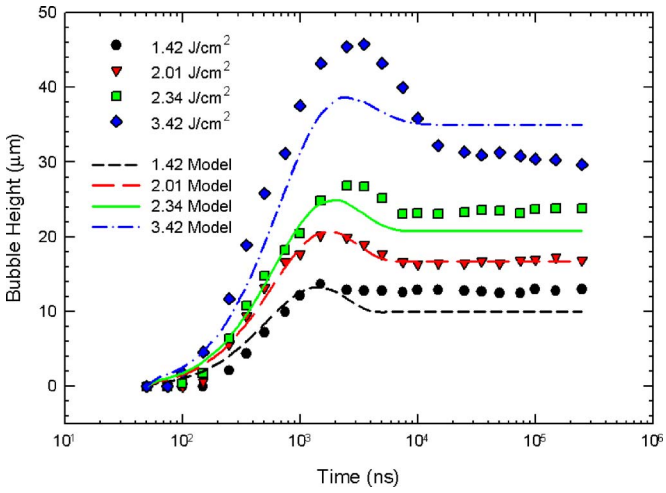

FIG. 5. Bubble growth data and model results for spot size of 30 μm and ink thickness of 50 μm.

$$P_{0,b} = P_{0,a}\left(\frac{E_b}{E_a}\right)\left(\frac{t_{i,a}}{t_{i,b}}\right)^{0.65\pm0.10}\left(\frac{d_a}{d_b}\right)^{0.39\pm0.12}, \tag{13}$$

where the error bars for m and n have been defined by the variations which increase the least-squares error by 10%.

Beginning with given process parameters, the bubble height as a function of time can be determined from numerical solution of Eq. (4). Such solutions were obtained using an initial value of y equal to the initial vapor-pocket thickness with an accompanying velocity of zero. In reality, the bubble height is initially zero, so that the initial vapor-pocket thickness was always subtracted from numerical bubble heights to correct for actual initial conditions.

Using the above expressions, we may fit the numerical solution based on Eq. (4) to a single data set so as to determine values of the ink density and viscous-force constant. Once these parameters have been evaluated, the above relations permit calculations of bubble growth for any other combination of ink thickness, beam diameter, and ablation energy.

IV. RESULTS AND DISCUSSION

A. Comparisons of experimental and predicted behaviors

The spot sizes selected for analysis of pure QS300 ink were 30 and 60 μm. Experiments were conducted for ink films coated using 0.5, 1, and 2 mil stainless steel shims, nominally corresponding to 12, 25, and 50 μm. For each combination of beam diameter and ink thickness, three fluences were chosen based on the highest fluence for which a bubble was observed, the lowest, and one value of fluence roughly halfway between the highest and lowest. Once parameters for every data set had been compiled, a differential equation solver was used to compute bubble growth curves for each case. Three of the six curves resulting from these computations are plotted along with their corresponding data sets averaged over 15 runs in Figs. 5–7. Error bars at the 68% confidence limit are shown for several individual data points in each figure.

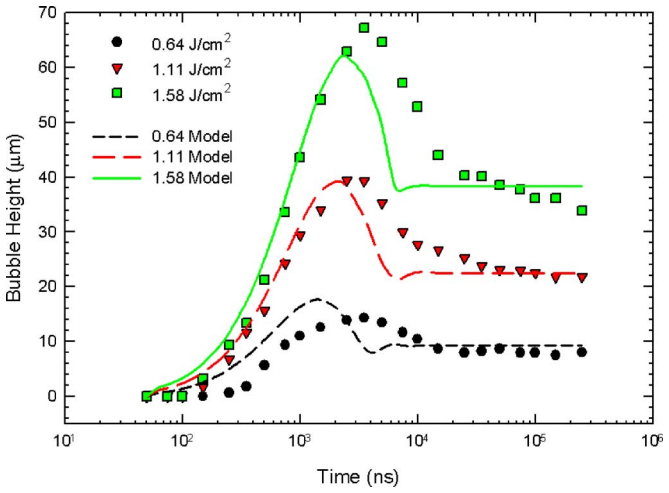

FIG. 6. Bubble growth data and model results for spot size of 60 μm and ink thickness of 50 μm.

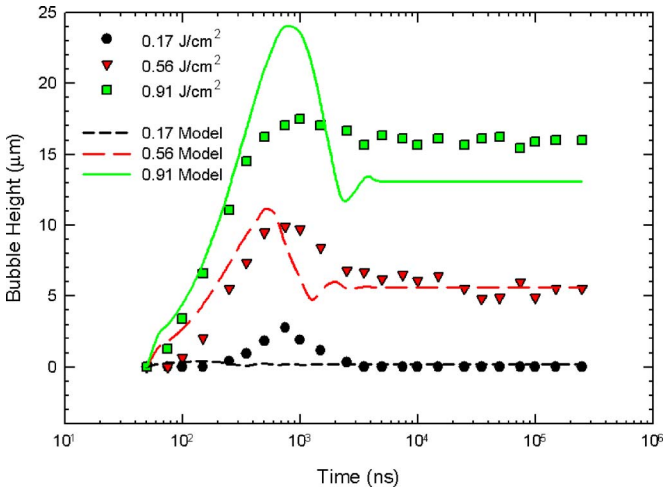

FIG. 7. Bubble growth data and model results for spot size of 30 μm and ink thickness of 12 μm.

In general, all bubble height versus time curves are characterized by rapid growth for a short period after laser irradiation. Rapid expansion indicates a large force in the direction of bubble growth. This force is a result of high pressure within the vapor pocket, which is created by the laser pulse. As the bubble expands, pressure is relieved and the bubble slows in its growth. Such inhibition can also arise from interfacial cooling and partial condensation of the vapor pocket.

Viscous forces combined with reduced vapor-pocket pressures participate in slowing bubble expansion, so that the bubble gradually reaches it maximum height. The peak bubble height is greater for an increased laser fluence, larger spot size, and thicker ink film. Once at its peak, the bubble height slowly relaxes to its final value. Some bubbles remain at their peak height, while others retract back toward the ink film. This retraction is most significant for bubbles produced with larger spot sizes and thicker ink films. Based on Figs. 5–7 deposition should be optimized when the bubble expands outward to a certain point and then retracts back toward its original position along the ink film.

The separation between ink film and substrate must be carefully selected based on the bubble size and shape. Because the bubble tip is round, the bubble radius varies greatly with height near the tip. Consequently, small shot-to-shot variations could cause chaotic depositions for ink-substrate gaps close to the expected bubble height. In comparison, by moving closer to the original ink-film surface, the bubble radius becomes much less sensitive to height. Hence, for gaps smaller than the expected bubble height, shot-to-shot variations should have less effect on deposition behavior. Consequently, repeatable depositions should prove more likely when the substrate is spaced at a distance less than the expected bubble height from the ink ribbon.

Based on Figs. 5–7 all bubbles begin expanding outward from the initial ink-film layer between 50 and 250 ns after the ablation pulse. These times are not noticeably affected by variations in laser spot size. According to these data, the determining factor for the beginning of bubble expansion is ink thickness. Bubble growth is evident for the 12 μm films from 50 to 100 ns after the laser pulse, whereas the 50 μm films begin growing anywhere from 100 to 250 ns following the laser pulse. Bubble heights peak anywhere from 750 ns after laser irradiation for small spot sizes and ink thicknesses to 3500 ns for large spot sizes and ink thicknesses.

From Figs. 5–7 we also conclude that relevant solutions to Eq. (4) agree reasonably well with bubble growth data. The data set used for baseline curve fitting is that shown in Fig. 5 (2.01 J/cm^2). As expected, the accuracy of the model deteriorates somewhat as process variables deviate further from those values used for curve fitting. Despite this mild deterioration, the model can be used quite efficaciously when comparing the most significant trends observed for bubble growth.

Before discussing positive and negative features of predictions from the model, we first consider dynamic effects arising from the three nonunity coefficients of the characteristic differential equation, labeled c_1, c_2, and c_3, as follows:

$$y'' + c_1 y' - c_2 y^{-1} = -c_3. \tag{14}$$

On this basis, parametric variations were conducted by varying only one coefficient and plotting curves of bubble height versus time. The generic effects from the three coefficients are illustrated in Fig. 8. These plots provide a qualitative visualization of the behavior associated with all three curve-fitting coefficients, which are each varied by ±20%. Based on these results, the first coefficient, c_1, affects only the system overshoot. By increasing c_1, the overshoot decreases and the system reaches its final height with less oscillation, as shown in Fig. 8(a).

Although the second coefficient, c_2, has little effect on the time required to reach the maximum bubble height, it greatly affects these values, as illustrated in Fig. 8(b). The entire bubble growth curve seems to shift upward in proportion to the magnitude of c_2. Final heights shift according to Eq. (9) for changes in both c_2 and c_3. Although the final height is shifted inversely by the value of c_3, bubble heights occurring prior to the peak do not change substantially. Changes in peak height are somewhat moderated in comparison to changes in final height, as shown in Fig. 8(c).

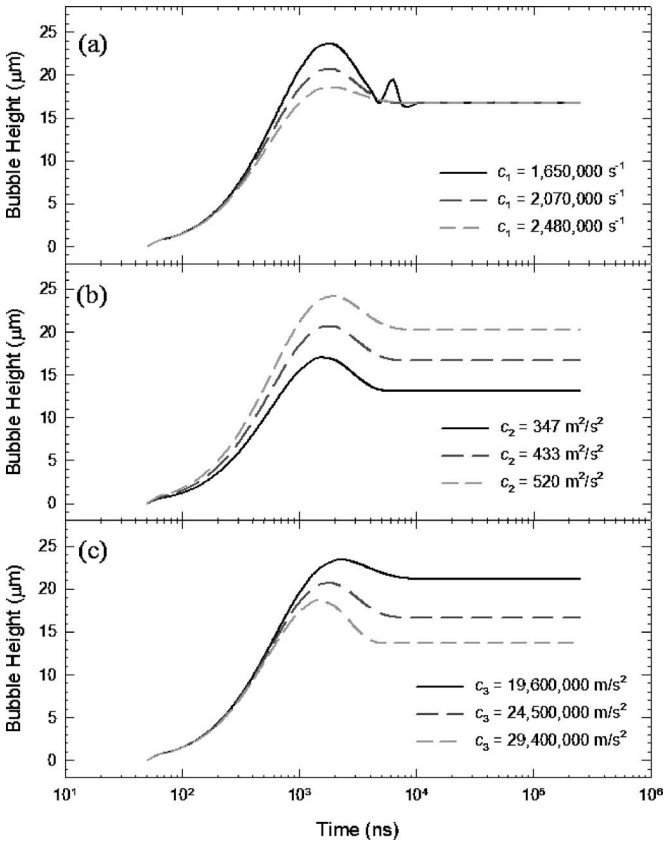

FIG. 8. Effects of variations in (a) first, (b) second, and (c) third coefficients of Eq. (14) on projected bubble growth. Coefficient values correspond to a spot size of 30 μm and an ink thickness of 50 μm.

An important trend that the model estimates well is the amount of retraction from the peak bubble height. Bubbles created with larger beam diameters show greater amounts of retraction. This trend is not as pronounced experimentally as the model predicts for smaller ink thicknesses, but the model, nevertheless, captures the general idea. Contrary to data, however, the model predicts an increase in this retraction with decreasing ink thickness. A potential cause for this discrepancy is our calculation of initial vapor-pocket size. If predicted values of initial vapor-pocket radius are too large, then the value of c_1 is too small. As c_1 drops, the amount of overshoot rises. In addition, if c_1 is incorrectly related to the initial vapor-pocket radius, this same error might be observed in the predictions.

The model predicts initial bubble growth quite well, especially for results obtained using a smaller beam diameter. For larger beam diameters, the error associated with initial bubble growth increases as the ink thickness drops with respect to the curve-fitted ink thickness of 50 μm. Based on the individual behavior associated with each coefficient, initial bubble growth errors could be caused by either an inaccurate ink density or an inaccurate value of c_2 [see Fig. 8(b)]. Direct interpretation of this error is difficult owing to the multiple relations embedded within the three coefficients of Eq. (14).

At this point, the efficacy of the proposed model can be partially assessed by combining Eq. (5) with Eq. (14) for steady-state conditions, thus obtaining

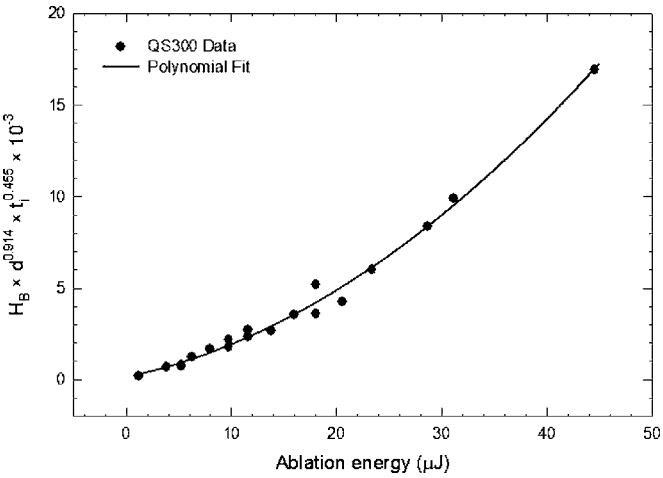

FIG. 9. Correlation for maximum bubble height with respect to beam diameter, ink thickness, and laser energy. The beam diameter d and ink thickness t_i are divided by 1 μm to ensure proper dimensionality.

$$y_{ss} = \frac{c_2}{c_3} = \frac{P_0 t_{\nu 0}}{P_{\text{atm}}}, \tag{15}$$

which eliminates any requirement for knowledge of the ink density. From Fig. 8, typical values for c_2 and c_3 are 500 m^2/s^2 and 2.5×10^7 m/s^2, respectively. Hence, given an initial vapor-pocket thickness of 1 μm, we find that the initial vapor-pocket pressure is $\sim$2 MPa, which is certainly not unreasonable. However, owing to the simplicity of the proposed model, which requires an estimate for $t_{\nu 0}$, physically meaningful values for model parameters properly await a more advanced model, as will be discussed further in Sec. V.

B. Correlations for bubble height, radius, and velocity

Future applications of MAPLE-DW require that we guarantee bubbles of a certain size; hence, we sought empirical relations between measured bubble dimensions and different combinations of laser energy, beam diameter, and ink thickness. A suitable representation linking maximum bubble height H_B to beam diameter d, ink thickness t_i, and laser energy E, is shown in Fig. 9. This relation was determined by first maximizing the correlation coefficient to determine exponents for beam diameter and ink thickness. Once these exponents were determined, a least-squares fit was used to determine the coefficients for a second-order polynomial in beam energy. Maximum bubble height, beam diameter, and ink thickness are given in micrometers, while the laser pulse energy is given in microjoules. On this basis, a polynomial correlation for maximum bubble height is given by

$$H_B = \frac{1}{d^{0.914} t_i^{0.455}}(134.4 + 123.6E + 5.7E^2), \tag{16}$$

where d and t_i have been divided by 1 μm, thus making them properly dimensionless. The correlation coefficient for QS300 when using Eq. (16) is 0.991. Uncertainties in the exponents for beam diameter and ink thickness are both $\pm$0.007, as defined by variations that increase the least-squares error by 10%.

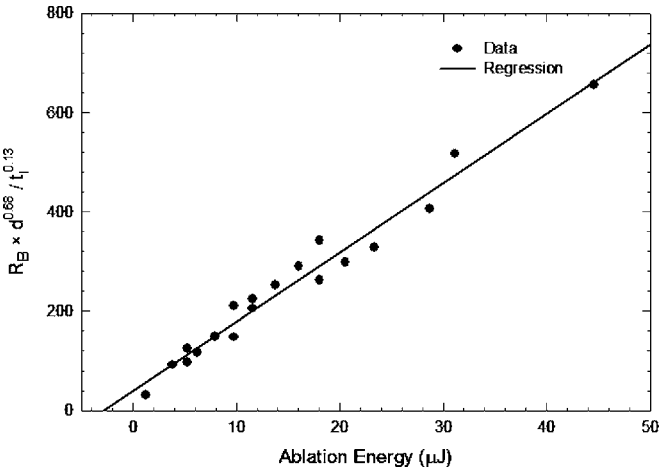

FIG. 10. Correlation for maximum bubble radius with respect to beam diameter, ink thickness, and laser energy. The beam diameter d and ink thickness t_i are divided by 1 μm to ensure proper dimensionality.

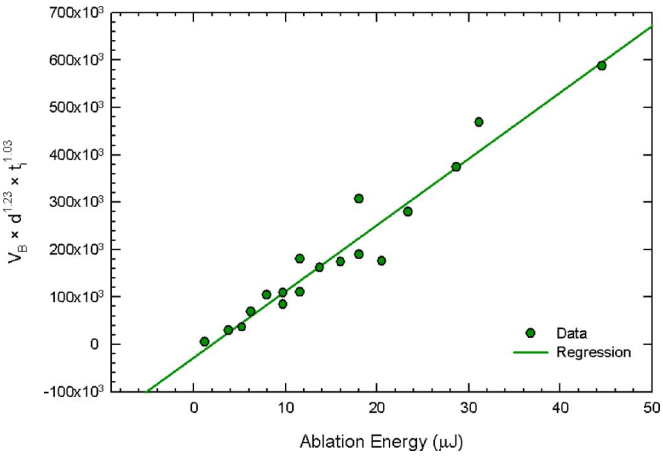

FIG. 11. Correlation for maximum bubble velocity with respect to beam diameter, ink thickness, and laser energy. The beam diameter d and ink thickness t_i are divided by 1 μm to ensure proper dimensionality.

As for the maximum bubble height, by investigating different relations combining ink thickness, beam diameter, and laser energy, we obtained a related expression for the bubble radius. The resulting equation was developed by using a least-squares fit of bubble radius data to parametric functions of the above process variables. Employing methods similar to those used to determine the coefficients for Eq. (16), the final relation specifying bubble radius, in micrometers, is given by

$$R_B = \frac{t_i^{0.13}}{d^{0.68}}(39.9 + 14.0E), \tag{17}$$

where d and t_i again represent dimensionless beam diameter and ink thickness, respectively. Figure 10 shows a comparison between the predictions from Eq. (17) and actual bubble radius data. The uncertainties in the exponents for beam diameter and ink thickness were both ±0.01, as defined again by independent variations which increase the least-squares error by 10%. The correlation coefficient for this linear relation is 0.97.

Given Eqs. (16) and (17), the corresponding maximum bubble height and radius can be estimated for any thickness of pure QS300 ink based on the energy and diameter of the vaporizing laser. Though these relations are imperfect, they provide a good starting point when estimating the required gap between the substrate and ink film for optimal deposition.

To understand further the dynamics of ink ablation and deposition, we examine next the velocity of bubble expansion. In particular, we determine the maximum bubble velocity from derivatives of Lagrange interpolating polynomials for every four data points.[6] As for the approach used to correlate maximum bubble height and radius to process variables, a similar correlation was applied to relate maximum bubble velocity to beam diameter, ink thickness, and laser energy. The result for this linear correlation is shown in Fig. 11. On this basis, the maximum bubble velocity can be specified, in m/s, by

$$V_B = \frac{1}{d^{1.23} t_i^{1.03}}(-27\,100 + 14\,000E), \tag{18}$$

where the laser energy is given in microjoules, while the beam diameter and ink thickness are again dimensionless, owing to division by 1 μm. The uncertainties of the exponents for beam diameter and ink thickness are both ±0.02, as defined by changes in value which increase the least-squares error by 10%. The correlation coefficient for this linear relation is 0.95.

For thicker ink films, the maximum bubble velocity drops, owing to an increased amount of material that resists bubble expansion. On the other hand, for a greater ink thickness, the plume threshold becomes much less sensitive to changes in laser spot size. Consequently, by increasing the beam diameter, the irradiance drops, which vaporizes less material. Less vaporization leads to a smaller pressure pulse, which accordingly reduces the maximum bubble velocity.

The combination of effects from ink thickness and beam diameter is difficult to visualize. Therefore, the maximum bubble velocity has been plotted in Fig. 12 against terms in Eq. (18) that include both of these variables. The front velocity is shown for both maximum and minimum bubble-generating fluences at each combination of ink thickness and beam diameter. A noticeable rise in front velocity occurs near the middle of this plot, indicating a potential maximum. If a maximum in front velocity exists at the center of Fig. 12, it would correspond to an ink thickness of ~25 μm and a beam diameter between 30 and 60 μm.

V. CONCLUSIONS

Three different regimes of laser-ink interaction were identified for the MAPLE-DW process: bubble, jet, and plume. By combining temporal images with deposition results, we found that the bubble regime is best for writing clean, repeatable patterns on substrates. Full data sets were thus collected to characterize bubble growth versus time for three different ink-film thicknesses of 12, 25, and 50 μm and for two laser-beam diameters of 30 and 60 μm. The laser

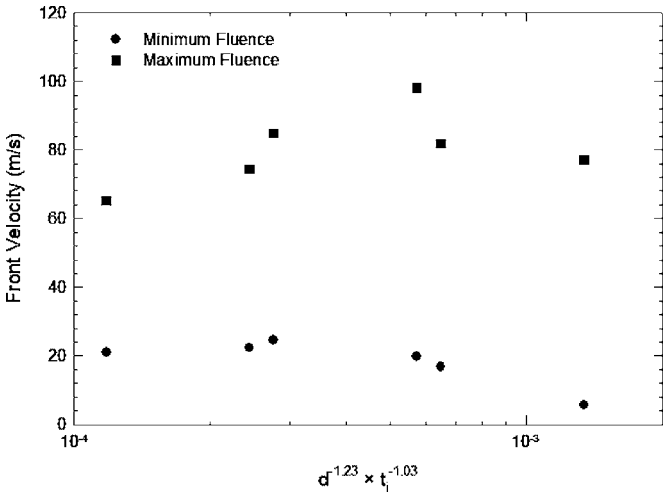

FIG. 12. Maximum bubble velocity at maximum and minimum laser fluences for each combination of beam diameter and ink thickness. The beam diameter d and ink thickness t_i are divided by 1 μm to ensure proper dimensionality.

fluences used for these data sets spanned the range of bubble-producing energies for each set of experimental conditions.

A simple force balance was applied to generate a differential equation for bubble growth based on both intermediate variables and known process parameters. Employing theoretical relations and suitable approximations, the intermediate variables were related to these process parameters. On this basis, bubble height verus time curves were determined and compared to the measured bubble data, as obtained via planar laser imaging.

The ink density obtained via the curve-fitting procedure was significantly lower than that expected based on the high metallic content of QS300 ink, even when accounting for the larger, cylindrical volume of ink assumed in the model. Ultimately, predictions of bubble height versus time were reasonably accurate considering the approximations made during the modeling process. Although our simplified model was based on a straightforward balance between vapor-pocket pressure and viscous forces, it nevertheless adequately predicts heights to which bubbles rise owing to vapor-pocket expansion—although less so for smaller ink thicknesses.

Correlations were developed to predict peak bubble height and bubble radius based on beam diameter, ink thickness, and laser energy. A correlation for the maximum bubble velocity was also developed using these same process parameters. All three correlations relate the desired quantity to a first multiplicand defined by the dimensionless beam diameter and ink thickness and a second multiplicand containing the laser energy. Based on these correlations, we suggest that optimal deposition should be achieved when bubbles expand outward, touch the substrate to deposit a small amount of ink, and then retract back towards the original ink film. This behavior is most often observed for larger beam diameters and thicker ink films.

The model presented in this paper successfully captures the dominant features of bubble development and expansion, followed by collapse to a presumably steady-state displacement. However, a number of assumptions and simplifications in the model lead to disagreement between measured and observed bubble heights. For example, the assumed constant viscosity fails to capture the shear-thinning behavior of the thick-film ink used in this research, which was specifically designed to facilitate screen-printing processes.[7] By including this behavior in the model, we might be able to understand why the bubble does not eventually regain its initial shape. In addition, the existing model does not account for surface tension effects, which may contribute to bubble retraction. Figure 2, in fact, demonstrates the presence of surface tension as the bubble collapses to a jet at higher fluences. The current model captures such forces driving bubble collapse by solely invoking a negative gauge pressure arising from vapor-pocket expansion. Further investigation is also needed on the efficacy of a 1 μm initial vapor-pocket thickness for the existing model.

In summary, we have investigated the MAPLE-DW process in the bubble regime via planar laser imaging and have proposed a simplified theoretical model to represent bubble growth trends. Correlations have been developed, which provide adequate approximations of maximum bubble height, bubble radius, and maximum bubble velocity. While future studies might lead to improved correlations, the relations developed in this work are probably sufficient for applying the MAPLE-DW process on an industrial scale. A more sophisticated model incorporating both varying viscosity and surface tension effects is currently under development. Presumably, a more robust model will lead to a better representation of bubble geometry, a more accurate value of ink density, and thus improved predictions of bubble height versus time.

ACKNOWLEDGMENTS

This project was supported by the Indiana 21st Century Research and Technology Fund. Two of the authors (B.R.L. and E.C.K.) acknowledge additional support from Lozar Student Fellowships.

[1] A. Piqué, B. R. Ringeisen, D. B. Chrisey, R. Modi, H. D. Young, H. D. Wu, and R. C. Y. Auyeung, *CLEO Conference on Lasers Electro-Optics*, Vol. 1, pp. 50-51, Chiba, Japan (2001).
[2] A. Piqué, D. B. Chrisey, J. M. Fitz-Gerald, and R. A. McGill, J. Mater. Res. **15**, 872 (2000).
[3] C. B. Arnold, T. E. Sutto, H. Kim, and A. Piqué, Laser Focus World **40**, S9 (2004).
[4] D. Young, R. C. Y. Auyeung, A. Piqué, D. B. Chrisey, and D. D. Dlott, Appl. Surf. Sci. **197–198**, 181 (2002).
[5] E. Kreysig, *Advanced Engineering Mathematics*, 8th ed. (Wiley, New York, 1999).
[6] E. W. Weisstein, *Lagrange Interpolating Polynomial*, in MathWorld, a Wolfram Web Resource, http://mathworld.wolfram.com/LagrangeInterpolatingPolynomial.html.
[7] R. W. Kay *et al.*, *Proceedings of Conference on MicroSystem Technologies*, Munich, Germany, 2003; see also J. J. Licari and L. R. Enlow, *Hybrid Microcircuit Technology Handbook* (Noyes, Westwood, NJ, 1998).